Title
Early Peak of Latent Heat Fluxes Regulates Diurnal Temperature Range in Montane Cloud Forests

Journal
Journal of Hydrometeorology, 22(9)

ISSN
1525-755X

Authors
Gu, Rong-Yu
Lo, Min-Hui
Liao, Chi-Ya
et al.

Publication Date
2021-07-14

DOI
10.1175/jhm-d-21-0005.1

Peer reviewed

Early Peak of Latent Heat Fluxes Regulates Diurnal Temperature Range in Montane Cloud Forests

Rong-Yu Gu[a], *Min-Hui Lo[a](minhuilo@ntu.edu.tw), Chi-Ya Liao[a,b], Yi-Shin Jang[a], Jehn-Yih Juang[c], Cho-Ying Huang[c], Shih-Chieh Chang[d], Cheng-I Hsieh[e], Yi-Ying Chen[f], Housen Chu[g], Kuang-Yu Chang[g]

[a] *Department of Atmospheric Sciences, National Taiwan University, Taipei, Taiwan*

[b] *Central Weather Bureau, Taipei, Taiwan*

[c] *Department of Geography, National Taiwan University, Taipei, Taiwan*

[d] *Department of Natural Resources and Environmental Studies, Center for Interdisciplinary Research on Ecology and Sustainability, National Dong Hwa University, Hualien, Taiwan*

[e] *Department of Bioenvironmental Systems Engineering, National Taiwan University, Taipei, Taiwan*

[f] *Research Center for Environmental Changes, Academia Sinica, Taipei, Taiwan*

[g] *Lawrence Berkeley National Laboratory, University of California, California, USA*

**Corresponding author*: Min-Hui Lo (minhuilo@ntu.edu.tw)

ABSTRACT

Hydro-climate in the montane cloud forest (MCF) regions is unique for its frequent fog occurrence and abundant water interception by tree canopies. Latent heat (LH) flux, the energy flux associated with evapotranspiration (ET), plays an essential role in modulating energy and hydrological cycles. However, how LH flux is partitioned between transpiration (stomatal evaporation) and evaporation (non-stomatal evaporation), and how it impacts local hydro-climate remain unclear. In this study, we investigate how fog modulates the energy and hydrological cycles of MCF by using a combination of in-situ observations and model simulations. We compare LH flux and associated micrometeorological conditions at two eddy-covariance sites—Chi-Lan (CL), a MCF, and Lien-Hua-Chih (LHC), a non-cloud forest in Taiwan. The comparison between the two sites reveals an asymmetric LH flux with an early peak at 9:00 in CL as opposed to LHC, where LH flux peaks at noon. The early peak of LH flux and its evaporative cooling dampen the increase in near-surface temperature during the morning hours in CL. The relatively small diurnal temperature range, abundant moisture brought by the valley wind, and local ET result in frequent afternoon fog formation. Fog water is then intercepted by the canopy, sustaining moist conditions throughout the night. To further illustrate this hydrological feedback, we used a land surface model to simulate how varying canopy water interception can affect surface energy and moisture budgets. Our study highlights the unique hydro-climatological cycle in MCF and, specifically, the inseparable relationship between the canopy and near-surface meteorology during the diurnal cycle.

Keywords: latent heat flux, canopy water, canopy evaporation, montane cloud forest, fog, diurnal temperature range

1. Introduction

Hydro-climate in the MCF regions is unique. Such forests can release large amounts of water vapor into the atmosphere via ET from a canopy made wet by frequent cloud immersion in montane regions (Bonan 2008; Gentine et al. 2019; Forzieri et al. 2020). Frequent fog occurrences in the MCFs provide 5% to 75% of the water source to the ecosystem as horizontal precipitation (Bruijnzeel et al. 2011a). This extra moisture is pivotal for providing an essential water source for the ecosystem, creating a unique physical setting that harbors diverse endemic species (Bruijnzeel et al. 2011a; Goldsmith et al. 2013; Bubb et al. 2004; Chang et al. 2002; Bruijnzeel 2000). Under such humid conditions, the ratio of ET to precipitation could be as low as 33% of the global forest average (Baldocchi and Ryu 2011; Chu et al. 2014). Recently, MCFs face a risk of lifting cloud base height due to elevated temperatures associated with increasing CO_2 concentration or anthropogenic forcing (Foster 2001; Oliveira et al. 2014; Williams et al. 2015; Still et al. 1999; Nair et al. 2003). Understanding the relationship between ET and fog may improve water cycle projections under changing fog frequency in the MCFs.

Generally, soil moisture-precipitation feedback indicates interaction between land and atmosphere through surface fluxes and boundary layer development; the feedback often occurs on daily to monthly time scales (Findell and Eltahir 1997; Koster et al. 2004; D'Odorico and Porporato 2004; Wang-Erlandsson et al. 2014; Shukla and Mintz 1982). Alterations in the local latent heat (LH) flux can impact the atmosphere, influencing soil moisture-precipitation interactions (Santanello Jr et al. 2018). The LH flux consists of transpiration, soil evaporation and canopy evaporation. Different partitioning in total LH flux can influence the time scale of atmospheric moisture recycling in the MCFs

(Wang et al. 2006; Wang-Erlandsson et al. 2014; Lawrence et al. 2007; Giambelluca et al. 2009; Chu et al. 2014). The reaction of transpiration to precipitation occurs slowly, roughly on monthly time scales, involving soil infiltration (related to soil texture) and plant water-use strategies (depending on atmospheric water vapor demand and plant species) (Wang-Erlandsson et al. 2014; Cavanaugh et al. 2011; Meinzer et al. 2004). Moreover, in MCFs, water interception by the canopy is much greater compared to other forested ecosystems due to frequent fog, implying canopy evaporation may dominate the LH flux (Lin et al. 2020; Bruijnzeel et al. 2011a; Bruijnzeel 2000; Chu et al. 2014; Giambelluca et al. 2009). However, accurately measuring and robustly modeling the canopy interception remains a challenge, especially in humid regions (Carlyle-Moses and Gash 2011; Friesen et al. 2015). Consequently, how the partition of LH flux impacts daily local hydro-climate in MCFs remains unclear.

Previous studies investigating the relationship between fog and LH flux in Taiwan's MCF regions focused primarily on the unidirectional effects of fog on total LH flux (Klemm et al. 2006; Mildenberger et al. 2009; Chu et al. 2014; Lin et al. 2020). Taiwan's MCFs are largely located at 1500 m to 2500 m a.s.l. The fog is associated with orographic lifting of moist air (Schulz et al. 2017). Chang et al. (2006) indicated that given certain visibility but increasing wind speed, fog deposition linearly increases because a droplet's path is more likely to be intersected by the canopy. During fog events, solar radiation is attenuated, leading to the suppression of both latent heat and sensible heat fluxes (Fig. S1; Klemm et al. 2006; Mildenberger et al. 2009). Such reduction of fluxes by fog can also be seen in Amazonian rainforests and other MCFs (Anber et al. 2015; Reinhardt and Smith 2008; Bruijnzeel et al. 2011). Although solar radiation weakens with fog deposition, LH flux is still positive but with relatively lower values than fog-free periods (Beiderwieden et al. 2008).

Based on eddy-covariance flux measurements, Chu et al. (2014) reported a unique "asymmetric LH flux" pattern at a cloud forest. LH flux was asymmetrically higher in the morning than in the afternoon. Without a robust means to quantify the canopy interception, they suggested that this asymmetric LH flux was likely created by morning canopy evaporation. Our study aims to revisit this "asymmetric LH flux" phenomenon by utilizing a combination of observations and model simulations. We used a land surface model to diagnose the complex partitioning of the terms contributing to the LH flux, and analyzed the meteorological data from flux tower observations in the CL MCF and LHC non-cloud forest (Fig. 1a) to support the aforementioned hypothesis. Several land surface model experiments were conducted to examine canopy water's contribution to the peak of LH flux in the CL MCF. We further investigated how the asymmetric diurnal cycle in the LH flux in the CL forest affects daily local hydro-climate, and explored causality among fog deposition, canopy evaporation, and asymmetric LH flux.

2. Materials and Methods

A combination of observations and model simulations was adopted. First, datasets from two flux towers in Taiwan's montane regions were compared to examine the relationship between LH flux and daily local hydro-climate. Characterized by frequent afternoon fog, the CL site is located within a cloud forest that experiences minimal human interference (Fig. 1b; Mildenberger et al. 2009; Chu et al. 2014). The LHC site, where fog seldom occurs, was used as a reference for non-cloud forest sites (Chen and Li 2012). Offline modeling experiments were performed to distinguish the most important physical processes in determining LH flux in montane forests in CL.

a. Site description

Located in northeastern Taiwan, the CL flux tower (24˚35'N, 121˚25'E) is at 1,650 m a.s.l.. Characterized by coniferous plantation forests, the site is dominated by Taiwan yellow cypress (Chamaecyparis obtuse var. formosana) ranging from 11 to 13 m in height (Chu et al. 2014; Lai et al. 2020). According to Chu et al. (2014), the tree trunk diameter at breast height (DBH) in 2008 was $20.4 \pm 6.0\mathrm{cm}$ $(\mathrm{DBH} > 10\mathrm{cm})$. The leaf area index (LAI) ranged from 3.3 to 5.7 m^2 m^{-2}, based on our monthly observations from 2015 to 2017. The 25 meters height flux tower was built on a 14˚ mountain sloping down to the southeast. Fog associated with upslope lifting leading to water condensation usually occurs in the afternoon (Fig. 1b). During the period from 2008 to 2011, foggy afternoon conditions occurred about 33% of the time, with longer foggy durations in winter due to northeast monsoon-instigated stratus cloud coverage. Additionally, annual mean temperature is usually 15 ˚C, while annual precipitation is around 3,915 mm; precipitation type varies among seasons. During summer, the local circulation dominates and the valley wind brings warm and humid air. The precipitation usually results from orographic lifting. This region may also experience heavy rain due to tropical cyclones, plum rains in summer, and precipitation induced by cold frontal lifting in winter (Klemm et al. 2006; Chu et al. 2014).

The LHC site (23˚55'N, 120˚53'E) is located in central Taiwan at an elevation of about 780 m a.s.l. A non-cloud forest, this site is dominated by mixed evergreen broadleaved trees with a mean canopy height of 17m. During growing seasons, the LAI can range from 2.5 to 4.5 m^2 m^{-2} (unpublished data). Maximum storage capacity in LHC ranges from 0.91 mm to 1.86 mm, depending on dry or wet seasons (Chen and Li 2016). A 25 meters height flux tower was built on top of a ridge in sub-watershed No.5 at the LHC Research Center (Chen and Li 2012). According to meteorological observations from 2009 to 2013, the annual average temperature is around 19°C and the annual precipitation is about 2,264 mm. This region may experience drought during winter because it is on the lee side of the prevailing winter monsoon (Chen and Li 2012).

b. Observational datasets

To understand the effects of the asymmetric LH flux on near-surface hydro-climate, we compared the fluxes and meteorological measurements from the CL and LHC flux towers. CL observations from 2008 to 2011 were compared with LHC observations made from 2009 to 2013. The incomplete overlap of observational periods can be attributed to the collapse of the CL flux tower due to a typhoon in 2012.

1) Meteorological observations

In both CL and LHC, temperature, relative humidity, and wind field measurements were implemented at the top of the flux towers; a rain gauge was installed 25 m from the tower (see Chu et al. (2014) and Chen and Li (2012) for details). A visibility sensor (Mira 3544, Aanderaa Data Inst., Bergen, Norway) was installed on top of the CL tower. The visibility of less than 1km can be defined as fog signal by referring to the World Meteorological Organization. Fog in CL usually occurs between 12:00 and 21:00 associated with valley wind (Fig. 1b; Fig. S1; Mildenberger et al. 2009; Klemm et al. 2006).

2) Flux measurements

In CL, an open-/closed-path eddy covariance system that includes a CSAT3 sonic anemometer (Campbell Sci., Inc. UT, USA), an open-path infrared gas analyzer (LI7500, LI-COR Biosciences, NE, USA), and a closed-path gas analyzer (LI7000, LICOR) was installed at a height of 24 m on the tower. Net radiation was measured by a CNR-1 net radiometer (Kipp & Zonen, Delft, The Netherlands) mounted on top of the tower. A RTD and a heater were included with the CNR-1 to measure the radiometer's internal temperature and to prevent condensation, respectively. Raw data such as three-dimensional velocity, sonic temperature, and water vapor concentration, were sampled at 10 Hz frequency and used to calculate 30-min LH flux, sensible heat flux and CO_2 flux. The data processing and QA/QC methodology applied follow Chu et al. (2014). According to Chen (2016), LH flux, sensible heat (SH) flux, and ground heat flux represent approximately 49%, 35%, and 0.6% of the net energy in the ecosystem, respectively. Energy balance closure (EBC) is evaluated by the following equation (1) (Papale et al. 2006; Stoy et al. 2013):

$$\mathrm{EBC} = \frac{LH + SH}{Rn - G - S} \tag{1}$$

where LH is latent heat flux, SH is sensible heat flux, Rn is net radiation, G is ground heat flux, and S is the storage term. The heat storage term is included in the quantification of the sensible heat flux during the measurement period. The vertical temperature profile was measured at nine different heights (0.4m, 2.0m, 3.6m, 5.2m, 8.0m, 13.2m, 16.0m, 18.0m, and 24.0m). T-type thermocouples are in 1Hz sample frequency and 2-minute averaging period. The heat storage of air is then calculated through the temperature difference over different layers of canopy volume. The annual averaged EBC is about 0.86. However, EBC is sometimes greater than 1 when wind direction shifts in the early morning. During the late afternoon when valley winds and fog are present, EBC is usually much lower (0.6-0.7) (Chen 2016). In addition, under foggy conditions, EBC tends to be around 0.7, indicating imbalances in the energy budget (Chen 2016). Since heat storage of air is included in the sensible heat flux, the lack of closure in the energy balance may result from other terms of heat storage, e.g., water or biomass (Moore and Fisch 1986). While imbalanced, our EBC is still within the typical range reported among FLUXNET sites (Wilson et al. 2002; Stoy et al. 2013).

In LHC forest, the earliest available flux data is from 2012. Fluxes were measured by an eddy covariance system, consisting of a sonic anemometer (81000, R. M. Young, MI, USA) and a LI7500 open-path infrared gas analyzer. The flux data was processed and quality-checked similar to CL. The EBC during the dry seasons is about 1, while that in the wet seasons is about 0.8 (Chen and Li 2012).

Potential evapotranspiration (PET, $W\ m^{-2}$) can be estimated for both CL and LHC by using the Penman-Monteith equation (Allen et al. 1998):

$$\lambda\mathrm{ET} = \frac{\Delta * (Rn - G) + \rho * C_p * VPD * g_a}{\Delta + \gamma(1 + g_a/g_c)}$$

where λ is the latent heat of vaporization, Δ is the slope of saturation vapor pressure temperature relationship ($\mathrm{mbar}\ ^{\circ}\mathrm{C}^{-1}$), ρ is the air density ($\mathrm{kg}\ m^{-3}$), C_p is the specific heat of air ($\mathrm{J}\ kg^{-1}\ K^{-1}$), VPD is the vapor pressure deficit (hPa), γ is the psychrometric constant ($\mathrm{hPa}\ ^{\circ}\mathrm{C}^{-1}$), g_a is the aerodynamic conductance ($m\ s^{-1}$), g_c is the canopy conductance ($m\ s^{-1}$). In our estimation of PET, we neglect G because it is a relatively small component in the LH flux partition, according to Klemm *et al* (2006) and Chen and Li (2012). Additionally, g_c is set to become infinity to imply a totally wet surface condition. The slope of saturation vapor pressure curve (Δ), the aerodynamic conductance (g_a), and the psychrometric constant (γ) were calculated based on formulas in Allen et al. (1998), while ρ can be calculated through:

$$\rho = \frac{P}{R_d * T_v}$$

where P is the pressure of the atmosphere (Pa), R_d is the gas constant of the dry air ($J kg^{-1} K^{-1}$), T_v is the virtual temperature ($\approx (1 + 0.608 q_v)$T) (K), and q_v is the specific humidity ($kg\ kg^{-1}$).

Furthermore, the Granier system's heat dissipation method (Granier 1985) is applied to obtain in-situ sap flow observations from June 2020 in the CL MCF. The diurnal cycle of sap flow density was analyzed to investigate whether transpiration is a major contributor to the asymmetry of LH flux (the aforementioned technical details see Supplemental Information).

3) Leaf wetness measurements

In CL, four leaf wetness sensors were set up at heights of 5.3 m, 8.3 m, 11.2 m, and 14.2 m (Chu et al. 2014). We analyzed the lower three sensors since they performed with more continuity and stability. A sensor threshold of 250 mV represented a dry canopy, while higher values represented the wet canopy. Differences of leaf wetness between sunrise and 3-hour after sunrise were calculated to demonstrate canopy wetness variation during the early morning. Note that 3-hour is the approximate time period when LH flux rises from sunrise until it reaches its peak. To determine the time of sunrise, solar radiation data from the CL flux tower was used, with sunrise being indicated by downward solar radiation exceeding 5 $W\, m^{-2}$ within 3:00 and 9:30. Results show that the sunrise timing is mainly around 5:30 to 7:00 in CL.

c. Model simulations

The Community Land Model (CLM, version 4 (Oleson et al. 2010)) in the Community

Earth System Model (CESM, version 1.0.3) was used to decompose the LH flux, with half-hourly observations in CL and LHC from 2008 to 2011 utilized as atmospheric forcing. These observations included 2 meter atmospheric temperature, atmospheric pressure, specific humidity, wind speed, precipitation, downward solar radiation and downward longwave radiation. CLM was chosen because LH flux partitioning bias was significantly improved in version 3.5 and the coupler-based system provided a convenient framework for discussing land-atmosphere interactions (Lawrence et al. 2007; Burns et al. 2018). Our modeling experiments were conducted as single-point simulations. The four years forcing ran repeatedly for a total of 24 years, with the last 8 years analyzed. Missing data in the atmospheric forcing was filled in with values from the climatological diurnal cycle for the corresponding month. Land cover type is prescribed as a 100% temperate evergreen needleleaf forest with a yearly-mean LAI of around 4.6. Six branches of Taiwan yellow cypress were taken from the CL and compare their weight between dry and totally wet conditions to obtain a coefficient of the maximum allowed canopy water of 0.2533 mm per unit of LAI. This experiment suggests that the maximum allowed canopy water of the whole forest in CL is 1.16 mm, which lies in the typical range of canopy storage capacity indicated by Bruijnzeel et al. (2011b). Bruijnzeel et al. (2011b) demonstrated that the water storage capacity above ground ranges from 0.38 mm of stand-level vegetation to 1.91 mm of all vegetation, including epiphytes. Although we do not have a corresponding observational value in CL, 1.16 mm of the canopy storage capacity is suitable for CL. The fog signal is included in the downward solar radiation forcing. However, the canopy in CLM does not capture this additional fog water because precipitation observations generally do not capture the horizontal fog deposition. To make the simulation more realistic, we added an additional precipitation forcing of 0.2 mm per 30 minutes when the fog occurred (observational visibility is less than 1km). This additional precipitation was based on the annual fog deposition rate measured by Chang et al. (2006) (the aforementioned technical details see Supplemental Information).

Two offline simulations, with and without canopy water storage scenarios (hereafter CTR and EXP, respectively), were conducted to demonstrate the impact of canopy water on the LH flux. In CTR, intercepted canopy water came from fog deposition, precipitation, or dew. Conversely, the canopy did not hold any water in EXP; water moved through the canopy and fell into the soil directly right after it formed or was intercepted on the canopy. Therefore, the model simulations may be used to demonstrate the role of canopy water on the total ET at a diurnal time scale. We also conducted three sensitivity tests for the canopy water effects, in which the atmospheric forcing and the land type are fixed as CTR, but the coefficient of the maximum allowed canopy water varied from 0.2533 (CTR) to 0.2 (max_cw_0.2), 0.1 (max_cw_0.1, default value in CLM), and 0.05 (max_cw_0.05), respectively.

After adding precipitation as the fog interception, the model simulated the same peak value of the LH flux as the observation (Fig. 2a). The model can explain about 70% variances of observational LH flux (Fig. 2b). However, there is a half-hour delay of the peak of LH flux in the models, 1.5 hours prior to that of net radiation. Thus, we claim that the model can capture the asymmetry of the diurnal cycle of the LH flux.

3. Results

a. The comparisons of LH fluxes and micrometeorological conditions between Chi-Lan (CL) and Lien-Hua-Chih (LHC) forests

An asymmetric diurnal cycle of LH flux with an early peak at 9:00 was observed in the CL MCF (Fig. 1c), which is not in phase with net radiation. The occurrence probability of daily maximum LH flux in CL is highly skewed (Fig. 1d). At the same time, that of net radiation is moderately skewed, suggesting that asymmetric LH flux cannot be explained by diurnal net radiation alone. In contrast, this phenomenon was not observed in the LHC non-cloud forest, where the occurrence probability of daily maximum LH flux is approximately symmetric.

The early-morning high LH flux in the CL MCF can modulate the increasing rate of the morning diurnal near-surface air temperature and provide an early water vapor source to the boundary layer. First, the air temperature increases more slowly in the morning since a large proportion of the energy is used to evaporate water (evapotranspiration). The value of PET is consistent with that of ET from 6:00 to 8:00 (Fig. 3), indicating that the land surface meets the evaporation demand of the atmosphere in the early morning. Thus, a smaller proportion of the energy is available to heat the near-surface atmosphere, reducing the diurnal temperature range to only about 2 ˚C in CL MCF. In contrast, the net energy gained in the LHC forest region is proportionally less distributed to ET; therefore, the diurnal temperature range is three times larger than CL (Fig. 4a). Second, the early peak of LH flux at 9:00 can provide local water vapor to the atmosphere. In addition to the local water vapor contribution, prevailing valley winds from dawn into the afternoon may bring water vapor from lowland forests to the flux towers (Fig. 4b; Fig. 4c). Although we cannot distinguish between advection and local contributions to total water vapor supply for the two sites, it is observed that specific humidity keeps increasing from 6:00 to 15:00 in both locations (Fig. 4b).

Because of the small diurnal temperature range in the CL, water vapor can easily reach saturated values by about 15:00. In contrast, in the LHC, the higher near-surface afternoon air temperatures prevent air saturation. Relative humidity (RH) usually keeps increasing from 7:00 to 17:00 in CL. The mean RH values of nearly 100% with small variations during the afternoon indicate frequent fog (Fig. 4d). The asymmetric pattern of LH flux does not vary much from season to season despite the smaller peak values of LH flux during winter (Fig. S2). Also, the characteristics of small diurnal temperature variations, water-vapor accumulation and prevailing valley wind during the daytime, as well as 100% RH at about 15:00 can be found in both summer and winter (Fig. S3).

The fog water may be intercepted by the canopy and become a source of canopy water. Because the RH remains high during the nighttime in CL, the intercepted fog water is likely to sustain until the next morning. Leaf wetness data indicates a significantly wetter canopy around the time of sunrise than 3-hour later (Table 1). This wet-dry contrast between sunrise and 3-hour after sunrise suggests that canopy water may substantially contribute to morning peak in LH flux.

b. Model simulations of the water and energy cycle in CL

CTR and EXP simulations were conducted to demonstrate the contribution of canopy water to the asymmetric LH flux. CTR is dedicated to representing the atmospheric and land condition in CL. At the same time, EXP shares the same land and atmospheric conditions as CTR, but no water can accumulate on the canopy. In the CTR simulation, canopy water accumulated in the afternoon and reached its peak at 6:00 (Fig. 5a), capturing the asymmetry of LH flux despite a half-hour delay of the peak in LH flux compared to observations. The EXP simulated a symmetric LH flux diurnal cycle with a peak at 10:30, the same phase as net radiation whose peak was at 11:00 (Fig. 5b). After decomposing the LH flux, we found that the early peak of LH flux in CTR was dominated by canopy evaporation, while the peak of LH flux in EXP was dominated by transpiration. In CTR, 71% of the LH flux was from canopy evaporation, and the peak in canopy evaporation was in phase with the drying trend of canopy water in the early morning. A sharp increase in canopy evaporation before 9:30, the peak timing of LH flux, resulted in an approximate 42% decrease in the canopy water within 3.5 hours after the sun rose. Transpiration in CTR was in phase with net radiation because of photosynthesis processes. Plants are energized by light to oxidize water, and this water and required minerals for photosynthesis rely on water pumped from roots to leaves. The amount of pumping water is correlated to air temperature, vapor pressure deficit, and available energy (Oren et al. 1999; Song et al. 2020). As the air temperature and net radiation peak around noon, transpiration also reached its peak around noon. However, the peak value of transpiration was about half that of the canopy evaporation. Thus, the early peak of LH flux can be attributed to high canopy evaporation peaking around 9:00 (Fig. 5c). Without the canopy water but with the same net radiation acquisition, EXP simulated a symmetric LH flux in which transpiration accounted for 83% of the total LH flux and the process dominated the surface energy budget partitioning (Fig. 5d).

4. Discussion

a. The diurnal LH flux and the fog under climate change: a risk or a benefit to the ecosystem in CL?

The small diurnal temperature range, frequent fog, precipitation, and plentiful canopy water play a vital role in regulating the water and energy cycle in CL, leading to the asymmetric LH flux. How these variables are affected by climate change and the corresponding response of hydro-climatology characteristics in the CL forest are worthy of further discussion. Firstly, the presence of the canopy water may result in the asymmetric LH flux. Our study shows that canopy water is a major contributor to the diurnal cycle's characteristics in hydro-climate in the MCFs. If canopy water is absent, most of the net radiation will warm up the canopy and near-surface atmosphere, as in the non-cloud forests. Also, if the canopy loses the ability to store the water or the water storage on the canopy is insufficient, the canopy evaporation in the early morning will become lower. In CL, the no-canopy scenario is unlikely to happen since the government has protected the region for several decades. Despite this, forest canopies' interception capacity may vary as a consequence of the changes in water input due to climate changes or changes of vegetation cover due to disturbance, management, or succession. From the perspective of land-atmosphere interactions, how the change in canopy water affects the partition of LH flux and even precipitation on longer timescales is worth more investigation.

Secondly, the amount of canopy water influences the asymmetry pattern of LH flux. In the MCFs, the canopy water in the early morning is derived from fog, dew, and precipitation accumulation since the previous afternoon or night. Recent studies have shown a decrease in fog frequency due to anthropogenic activities (Nair et al. 2003; Williams et al. 2015). Rising temperatures during the daytime might prevent water vapor saturation during the afternoon hours (Foster 2001; Still et al. 1999). In addition, nighttime temperatures may influence dew formation. The higher temperature at night will decrease RH and have negative impacts on condensation and dew formation. While the contribution of dew to canopy water decreases, the peak of canopy evaporation in the early morning might not so high as the present, thus causing symmetric LH flux and rising temperature in the daytime. Overall, the warming climate might have a negative impact on dew and fog formation. Furthermore, precipitation patterns may be altered as the climate changes through mechanisms such as the "wet get wetter and dry get drier" mechanism (Dore 2005; Chou et al. 2013; Lan et al. 2019). Changes in both precipitation frequency and intensity might impact the storage of canopy water (Foster 2001). Intense rainfall is more likely to happen in Taiwan based on 40-year of observations (Shiu et al. 2009). Decreases in light and low-intensity rainfall would reduce canopy interception, causing adverse effects to canopy evaporation (Dunkerley 2021; Magliano et al. 2019).

Diverse changes in temperature and RH in future projections and the complex topography in montane regions may also result in large uncertainties in local circulations (Still et al. 1999; Lin et al. 2015; Rangwala et al. 2012). Warming temperature and decreasing RH may lift the cloud base height (Williams et al. 2015). As the temperature gradient varies between the mountain top and valley, the wind magnitude changes. Changes in mountain-valley wind circulations might alter both precipitation and fog occurrence. However, the contribution of advection to the water vapor accumulation in the CL during the daytime remains unknown. Changes in advection might affect water vapor supply, which then impacts the fog or precipitation climatology, thus influencing the amount of canopy water. If the amount of canopy water is insufficient to support high canopy evaporation in the early morning, the diurnal cycle of the LH flux may become symmetric, peaking at noontime. Less canopy evaporation in the early morning from 6:00 to 9:00 would, in turn, increase the diurnal temperature range, implying higher afternoon temperatures are unfavorable for fog formation. Under the non-fog scenario, the loop in the schematic plot of Fig. 6 may not sustain and lead to less horizontal precipitation, creating a water stress environment.

Finally, despite concerns that the disappearance of fog may have negative impacts on the growth of plants and epiphytes community, a lack of fog might benefit Taiwan's MCFs (Foster 2001; Limm et al. 2012; Ball and Tzanopoulos 2020). In some seasonally dry regions, fog interception is essential to plant water use, especially to the top of the canopy. Research has found that fog could support tree growth because of their direct water use through foliar water uptake (Dawson and Goldsmith 2018; Limm et al. 2012). However, in Taiwan's MCFs, where annual precipitation usually exceeds 3000 mm, water may not be a limiting factor for tree growth. Even if fog disappears, wet leaves can still exist if the precipitation patterns do not change significantly. A lack of fog seems unlikely to negatively influence the available water for the trees but might substantially increase the available energy for photosynthesis or tree growth. Mildenberger et al. (2009) indicated fog could block about 64% of solar radiation. Without fog, the acquisition of solar energy and larger vapor pressure deficit might favor the opening of stomata and increase CO_2 uptake; however, this argument needs more exploration of the accompanied CO_2 flux and stomatal conductance from observation and models simulations.

b. The sap flow measurement and the sensitivity test of the maximum allowed canopy water

Previous studies have suggested that transpiration is the main content of ET, whose diurnal cycle tends to be symmetric in forests (Oren et al. 1998; Paul-Limoges et al. 2020; Burgess and Dawson 2004). However, in-situ sap flow observations have indicated that the transpiration peak timing is around noontime in CL cloud forest (Fig. 4c in Chu et al. (2014)), 3 hours later than the LH flux. The land surface model simulations further demonstrate the minor contribution of transpiration to the total LH, consistent with the sap flow measurement (Fig. 3, 5c; Fig. S4). The model simulations also imply that the asymmetry of diurnal LH flux may majorly result from canopy evaporation.

To examine the impact of the maximum allowed canopy water storage on the asymmetry of LH flux in CL, tests of the sensitivity to the coefficient of the maximum allowed canopy water were conducted. The coefficient of maximum allowed canopy water regulates the maximum allowed canopy water by multiplying the coefficient with LAI in the model. In our sensitivity test, the atmospheric forcing and the land type were fixed as CTR, but the coefficient of the maximum allowed canopy water was varied from 0.2533 (CTR) to 0.2 (max_cw_0.2), 0.1 (max_cw_0.1), and 0.05 (max_cw_0.05), respectively. These four simulations can capture the asymmetric LH flux with the peak sometime between 8:30 and 9:30. The early peaks of LH fluxes are all derived from canopy evaporation's peak values in the early morning. The canopy water in all simulations starts to increase in the afternoon, reaches a peak at dawn and then decreases before 9:00 (Fig. 7a). In these four simulations, the higher the maximum allowed canopy water is, the larger the peak of latent heat flux is (Fig. 7b). This indicates more water evaporates under the same available energy situation, but varying the coefficient of the maximum allowed canopy water will not significantly affect the asymmetry of LH flux (Fig. 7c).

c. The importance of fog description in models

Fog is a source of canopy water that contributes to the asymmetric LH flux. In atmospheric models, which do not include fog's effects on the energy and water cycle, the land will receive excess solar radiation, and the LH flux will be overestimated. Furthermore, CO_2 uptake in the cloud forest may be biased without fog. Under foggy conditions, the LH flux and CO_2 flux are reduced by approximately 56% and 48%, respectively (Table 2). As a result, ignoring fog formation and its effects on energy and water cycles may overestimate solar radiation and vapor pressure deficit, leading to increased LH and CO_2 fluxes in the MCFs.

Seasonal analysis demonstrates that surface fluxes are generally decreased by fog occurrence (Table 3). LH flux is most largely reduced by fog during autumn, and CO_2 flux is decreased dramatically by fog in summer. The results of fluxes in seasonal variation are worthy of discussing water and energy regulation on the surface fluxes, and the physical mechanism behind it deserves a future study.

5. Conclusion

The unique hydro-climatological cycle in CL MCF is summarized in Fig. 6, where the following characteristics are highlighted: (1) An early peak in the LH flux results in a slow increase in the near-surface temperature during the morning; (2) during the daytime, the valley wind brings water vapor from low elevations, combined with ET from the local forest, resulting in water vapor accumulation until 15:00; (3) because of the small diurnal temperature range, water vapor concentrations can easily reach saturation values during the afternoon resulting in fog formation. Fog further serves as a source of canopy water in addition to dew and precipitation; (4) plentiful canopy water is sustained throughout the night because of the high RH. After sunrise, the drying tendency in leaf wetness implies a critical role for canopy water in the early peak in LH flux. This unique hydro-climatological cycle in the MCFs reflects the inseparable relationship between the canopy and near-surface meteorology during the diurnal cycle. The unique cycle is observed in all seasons. The offline model simulations suggest the asymmetric LH flux is principally due to high canopy evaporation during the early morning.

In this study, where the water vapor comes from and how the asymmetric LH flux will be influenced by different atmospheric forcing as the climate changes remain uncertain. Future works may require isotopic measurements or the tracer model experiment to distinguish local and advected water vapor. In addition, since leaf wetness fails to measure the amount of canopy water, improved measurement in the time evolution of canopy water amount will improve understanding on how the canopy water varies in different environmental circumstances. Also, idealized model simulations may be needed to determine how each variable in the atmospheric forcing affects the hydro-climatological cycle in the MCFs. The offline CLM framework does not allow us to analyze how the asymmetric LH flux affects local climate. We, therefore, propose to utilize a single-column Community Atmosphere Model coupled CLM to explore how surface fluxes interact with temperature, boundary layer development, and cloud formation in the future.

Acknowledgements

We sincerely acknowledge Dr. Yen-Jen Lai, Dr. John Chun-Han Lin, Dr. Hao-Wei Wey, Ms. Li-Wei Chao, Mr. Jin-De Hwang, Mr. Yu-Hung Chang, Mr. Po-Shen Chang, as well as Ms. Yun-Ya Chu on discussing the cloud forest issue. We also thank Dr. Tomonori Kume and Ms. Sophie Laplace on advising the sap flow measurements. We also thank Prof. Ming-Hsu Li for fruitful discussions. We also thank Mr. Ren-Jie Wu, Ms. Tzu-Ying Yang and NTU COOK lab for the assistance on installing the sap flow measurements. This study was supported by the NTU Core Consortiums project and the MOST 106-2111-M-002-010-MY4 to National Taiwan University.

Data availability

Observational data from CL flux tower is provided by Dr. Jehn-Yih Juang and Dr. Shih-Chieh Chang, and the data from LHC flux tower is provided by Dr. Ming-Hsu Li and Dr. Yi-Ying Chen. Both CL and LHC flux tower data are available upon request. The land model simulations and the 30 minutes averaged sap flow data are compiled on the Zenodo data repository (https://doi.org/10.5281/zenodo.4092769). The topography data from 30-meter Shuttle Radar Topography Mission version 6.0 are download from National Oceanic and Atmospheric Administration ERDDAP data server (https://coastwatch.pfeg.noaa.gov/erddap/griddap/usgsCeSrtm30v6.html?fbclid=IwAR1oI58nlrquawJmwuULwgjWWIISzZWZAdg2eGfAKvA0NujP7WHzeZebMYY).

Code availability

CLM is the coupler-based land segment in the CESM. The CESM code is released http://www.cesm.ucar.edu/models/. Analyses except sap flow were conducted through MATLAB R2015a. Sap flow data were analyzed by using R version 3.6.3. All data were visualized by using MATLAB R2015a. Codes for analyses are available from the authors upon request.

REFERENCES

Allen, R. G., L. S.Pereira, D.Raes, and M.Smith, 1998: Crop evapotranspiration-Guidelines for computing crop water requirements-FAO Irrigation and drainage paper 56. *Fao, Rome*, **300**, D05109.

Anber, U., P.Gentine, S.Wang, and A. H.Sobel, 2015: Fog and rain in the Amazon. *Proc. Natl. Acad. Sci. U. S. A.*, **112**, 11473–11477, https://doi.org/10.1073/pnas.1505077112.

Baldocchi, D. D., and Y.Ryu, 2011: A synthesis of forest evaporation fluxes–from days to years–as measured with eddy covariance. *Forest Hydrology and Biogeochemistry*, Springer, 101–116.

Ball, L., and J.Tzanopoulos, 2020: Interplay between topography, fog and vegetation in the central South Arabian mountains revealed using a novel Landsat fog detection technique. *Remote Sens. Ecol. Conserv.*, **6**, 498–513, https://doi.org/10.1002/rse2.151.

Beiderwieden, E., V.Wolff, Y.Hsia, and O.Klemm, 2008: It goes both ways: measurements of simultaneous evapotranspiration and fog droplet deposition at a montane cloud forest. *Hydrol. Process.*, **22**, 4181–4189.

Bonan, G. B., 2008: Forests and climate change: forcings, feedbacks, and the climate benefits of forests. *Science (80-.).*, **320**, 1444–1449.

Bruijnzeel, L. A., 2000: Hydrology of tropical montane cloud forests: a re-evaluation. *Proc. Second Int. Colloq. Hydrol. Humid Trop.*, **1**, 1–18.

Bruijnzeel, L. A., M.Mulligan, and F. N.Scatena, 2011a: *Hydrometeorology of tropical montane cloud forests: Emerging patterns*. 465–498pp.

Bruijnzeel, L. A., F. N.Scatena, and L. S.Hamilton, 2011b: *Tropical montane cloud forests: science for conservation and management*. Cambridge University Press,.

Bubb, P., I. A.May, L.Miles, and J.Sayer, 2004: Cloud forest agenda.

Burgess, S. S. O., and T. E.Dawson, 2004: The contribution of fog to the water relations of Sequoia sempervirens (D. Don): foliar uptake and prevention of dehydration. *Plant. Cell Environ.*, **27**, 1023–1034.

Burns, S. P., S. C.Swenson, W. R.Wieder, D. M.Lawrence, G. B.Bonan, J. F.Knowles, and P. D.Blanken, 2018: A Comparison of the Diel Cycle of Modeled and Measured Latent Heat Flux During the Warm Season in a Colorado Subalpine Forest. *J. Adv. Model. Earth Syst.*, **10**, 617–651, https://doi.org/10.1002/2017MS001248.

Carlyle-Moses, D. E., and J. H. C.Gash, 2011: Rainfall interception loss by forest canopies. *Forest hydrology and biogeochemistry*, Springer, 407–423.

Cavanaugh, M. L., S. A.Kurc, and R. L.Scott, 2011: Evapotranspiration partitioning in semiarid shrubland ecosystems: a two-site evaluation of soil moisture control on transpiration. *Ecohydrology*, **4**, 671–681.

Chang, S.-C., I.-L.Lai, and J.-T.Wu, 2002: Estimation of fog deposition on epiphytic bryophytes in a subtropical montane forest ecosystem in northeastern Taiwan. *Atmos. Res.*, **64**, 159–167.

Chang, S. C., C. F.Yeh, M. J.Wu, Y. J.Hsia, and J. T.Wu, 2006: Quantifying fog water deposition by in situ exposure experiments in a mountainous coniferous forest in Taiwan. *For. Ecol. Manage.*, **224**, 11–18, https://doi.org/10.1016/j.foreco.2005.12.004.

Chen, C. Y., 2016: Investigating interannual and seasonal variations of energy balance in a mountain cloud forest in Chi-Lan Mountain (http://dx.doi.org/10.6342/NTU201603252) [Master Thesis, Department of Geography, National Taiwan University]. Airiti Library

Chen, Y. Y., and M. H.Li, 2012: Determining adequate averaging periods and reference coordinates for eddy covariance measurements of surface heat and water vapor fluxes over mountainous terrain. *Terr. Atmos. Ocean. Sci.*, **23**, 685–701, https://doi.org/10.3319/TAO.2012.05.02.01(Hy).

——, and——, 2016: Quantifying rainfall interception loss of a subtropical broadleaved forest in central Taiwan. *Water (Switzerland)*, **8**, 1–19, https://doi.org/10.3390/w8010014.

Chou, C., J. C. H.Chiang, C.-W.Lan, C.-H.Chung, Y.-C.Liao, and C.-J.Lee, 2013: Increase in the range between wet and dry season precipitation. *Nat. Geosci.*, **6**, 263–267.

Chu, H., and Coauthors, 2014: Does canopy wetness matter? Evapotranspiration from a subtropical montane cloud forest in Taiwan. *Hydrol. Process.*, **28**, 1190–1214.

D'Odorico, P., and A.Porporato, 2004: Preferential states in soil moisture and climate dynamics. *Proc. Natl. Acad. Sci.*, **101**, 8848–8851.

Dawson, T. E., and G. R.Goldsmith, 2018: The value of wet leaves. *New Phytol.*, **219**, 1156–1169, https://doi.org/10.1111/nph.15307.

Dore, M. H. I., 2005: Climate change and changes in global precipitation patterns: what do we know? *Environ. Int.*, **31**, 1167–1181.

Dunkerley, D. L., 2021: Light and low-intensity rainfalls: A review of their classification, occurrence, and importance in landsurface, ecological and environmental processes. *Earth-Science Rev.*, **214**, 103529, https://doi.org/10.1016/j.earscirev.2021.103529.

Findell, K. L., and E. A. B.Eltahir, 1997: An analysis of the soil moisture-rainfall feedback, based on direct observations from Illinois. *Water Resour. Res.*, **33**, 725–735.

Forzieri, G., and Coauthors, 2020: Increased control of vegetation on global terrestrial energy fluxes. *Nat. Clim. Chang.*, **10**, 356–362, https://doi.org/10.1038/s41558-020-0717-0.

Foster, P., 2001: The potential impacts of global climate change on tropical montane cloud forests. *Earth-Science Rev.*, **55**, 73–106, https://doi.org/10.1016/S0012-8252(01)00056-3.

Friesen, J., J.Lundquist, and J. T.VanStan, 2015: Evolution of forest precipitation water storage measurement methods. *Hydrol. Process.*, **29**, 2504–2520, https://doi.org/10.1002/hyp.10376.

Gentine, P., A.Massmann, B. R.Lintner, S.Hamed Alemohammad, R.Fu, J. K.Green, D.Kennedy, and J.Vilà-Guerau de Arellano, 2019: Land–atmosphere interactions in the tropics–a review. *Hydrol. Earth Syst. Sci.*, **23**.

Giambelluca, T. W., R. E.Martin, G. P.Asner, M.Huang, R. G.Mudd, M. A.Nullet, J. K.DeLay, and D.Foote, 2009: Evapotranspiration and energy balance of native wet montane cloud forest in Hawai ‘i. *Agric. For. Meteorol.*, **149**, 230–243.

Goldsmith, G. R., N. J.Matzke, and T. E.Dawson, 2013: The incidence and implications of clouds for cloud forest plant water relations. *Ecol. Lett.*, **16**, 307–314, https://doi.org/10.1111/ele.12039.

Granier, A., 1985: Une nouvelle méthode pour la mesure du flux de sève brute dans le tronc des arbres. *Annales des Sciences forestières*, Vol. 42of, EDP Sciences, 193–200.

Klemm, O., S. C.Chang, and Y. J.Hsia, 2006: Energy fluxes at a subtropical mountain cloud forest. *For. Ecol. Manage.*, **224**, 5–10, https://doi.org/10.1016/j.foreco.2005.12.003.

Koster, R. D., and Coauthors, 2004: Regions of strong coupling between soil moisture and precipitation. *Science (80-.).*, **305**, 1138–1140.

Lai, G.-Y., H.-C.Liu, A. J.Kuo, and C.Huang, 2020: Epiphytic bryophyte biomass estimation on tree trunks and upscaling in tropical montane cloud forests. *PeerJ*, **8**, e9351.

Lan, C.-W., M.-H.Lo, C.-A.Chen, and J.-Y.Yu, 2019: The mechanisms behind changes in the seasonality of global precipitation found in reanalysis products and CMIP5 simulations. *Clim. Dyn.*, **53**, 4173–4187.

Lawrence, D. M., P. E.Thornton, K. W.Oleson, and G. B.Bonan, 2007: The partitioning of evapotranspiration into transpiration, soil evaporation, and canopy evaporation in a GCM: Impacts on land-atmosphere interaction. *J. Hydrometeorol.*, **8**, 862–880, https://doi.org/10.1175/JHM596.1.

Limm, E., K.Simonin, and T.Dawson, 2012: Foliar uptake of fog in the coast redwood ecosystem: a novel drought-alleviation strategy shared by most redwood forest plants. *In: Standiford, Richard B.; Weller, Theodore J.; Piirto, Douglas D.; Stuart, John D., tech. coords. Proceedings of coast redwood forests in a changing California: A symposium for scientists and managers. Gen. Tech. Rep. PSW-GTR-238. Albany, CA: Pacific So*, Vol. 238of, 273–281.

Lin, B. S., H.Lei, M. C.Hu, S.Visessri, and C. I.Hsieh, 2020: Canopy Resistance and Estimation of Evapotranspiration above a Humid Cypress Forest. *Adv. Meteorol.*, **2020**, https://doi.org/10.1155/2020/4232138.

Lin, C. Y., Y. J.Chua, Y. F.Sheng, H. H.Hsu, C. T.Cheng, and Y. Y.Lin, 2015: Altitudinal and latitudinal dependence of future warming in Taiwan simulated by WRF nested with ECHAM5/MPIOM. *Int. J. Climatol.*, **35**, 1800–1809, https://doi.org/10.1002/joc.4118.

Magliano, P. N., J. I.Whitworth-Hulse, E. L.Florio, E. C.Aguirre, and L. J.Blanco, 2019:

Interception loss, throughfall and stemflow by Larrea divaricata: The role of rainfall characteristics and plant morphological attributes. *Ecol. Res.*, **34**, 753–764, https://doi.org/10.1111/1440-1703.12036.

Meinzer, F. C., S. A.James, and G.Goldstein, 2004: Dynamics of transpiration, sap flow and use of stored water in tropical forest canopy trees. *Tree Physiol.*, **24**, 901–909.

Mildenberger, K., E.Beiderwieden, Y.-J.Hsia, and O.Klemm, 2009: CO2 and water vapor fluxes above a subtropical mountain cloud forest—The effect of light conditions and fog. *Agric. For. Meteorol.*, **149**, 1730–1736.

Moore, C. J., and G.Fisch, 1986: Estimating heat storage in Amazonian tropical forest. *Agric. For. Meteorol.*, **38**, 147–168, https://doi.org/10.1016/0168-1923(86)90055-9.

Nair, U. S., R. O.Lawton, R. M.Welch, and R. A.Pielke, 2003: Impact of land use on Costa Rican tropical montane cloud forests: Sensitivity of cumulus cloud field characteristics to lowland deforestation. *J. Geophys. Res. Atmos.*, **108**, https://doi.org/10.1029/2001jd001135.

Oleson, K. W., and Coauthors, 2010: Technical description of version 4.0 of the Community Land Model (CLM).

Oliveira, R. S., C. B.Eller, P. R. L.Bittencourt, and M.Mulligan, 2014: The hydroclimatic and ecophysiological basis of cloud forest distributions under current and projected climates. *Ann. Bot.*, **113**, 909–920, https://doi.org/10.1093/aob/mcu060.

Oren, R., N.Phillips, G.Katul, B. E.Ewers, and D. E.Pataki, 1998: Scaling xylem sap flux and soil water balance and calculating variance: a method for partitioning water flux in forests. *Annales des Sciences Forestieres*, Vol. 55of, EDP Sciences, 191–216.

Oren, R., N.Phillips, B. E.Ewers, D. E.Pataki, and J. P.Megonigal, 1999: Sap-flux-scaled transpiration responses to light, vapor pressure deficit, and leaf area reduction in a flooded Taxodium distichum forest. *Tree Physiol.*, **19**, 337–347, https://doi.org/10.1093/treephys/19.6.337.

Papale, D., and Coauthors, 2006: Towards a standardized processing of Net Ecosystem Exchange measured with eddy covariance technique: algorithms and uncertainty estimation. *Biogeosciences*, **3**, 571–583.

Paul-Limoges, E., S.Wolf, F. D.Schneider, M.Longo, P.Moorcroft, M.Gharun, and A.Damm, 2020: Partitioning evapotranspiration with concurrent eddy covariance measurements in a mixed forest. *Agric. For. Meteorol.*, **280**, 107786.

Rangwala, I., J.Barsugli, K.Cozzetto, J.Neff, and J.Prairie, 2012: Mid-21st century projections in temperature extremes in the southern Colorado Rocky Mountains from regional climate models. *Clim. Dyn.*, **39**, 1823–1840, https://doi.org/10.1007/s00382-011-1282-z.

Reinhardt, K., and W. K.Smith, 2008: Impacts of cloud immersion on microclimate, photosynthesis and water relations of Abies fraseri (Pursh.) Poiret in a temperate mountain cloud forest. *Oecologia*, **158**, 229–238.

Santanello Jr, J. A., and Coauthors, 2018: Land–atmosphere interactions: The LoCo perspective. *Bull. Am. Meteorol. Soc.*, **99**, 1253–1272.

Schulz, H. M., C. F.Li, B.Thies, S. C.Chang, and J.Bendix, 2017: Mapping the montane cloud forest of Taiwan using 12 year MODIS-derived ground fog frequency data. *PLoS One*, **12**, 12–15, https://doi.org/10.1371/journal.pone.0172663.

Shiu, C. J., S. C.Liu, and J. P.Chen, 2009: Diurnally asymmetric trends of temperature, humidity, and precipitation in Taiwan. *J. Clim.*, **22**, 5635–5649, https://doi.org/10.1175/2009JCLI2514.1.

Shukla, J., and Y.Mintz, 1982: Influence of land-surface evapotranspiration on the earth's climate. *Science (80-.).*, **215**, 1498–1501.

Song, X., S.Lyu, and X.Wen, 2020: Limitation of soil moisture on the response of transpiration to vapor pressure deficit in a subtropical coniferous plantation subjected to seasonal drought. *J. Hydrol.*, **591**, 125301, https://doi.org/10.1016/j.jhydrol.2020.125301.

Still, C. J., P. N.Foster, and S. H.Schneider, 1999: Simulating the effects of climate change on tropical montane cloud forests. *Nature*, **398**, 608–610.

Stoy, P. C., and Coauthors, 2013: A data-driven analysis of energy balance closure across FLUXNET research sites: The role of landscape scale heterogeneity. *Agric. For. Meteorol.*, **171**, 137–152.

Wang-Erlandsson, L., R. J.Van DerEnt, L. J.Gordon, and H. H. G.Savenije, 2014: Contrasting roles of interception and transpiration in the hydrological cycle–Part 1: Temporal characteristics over land. *Earth Syst. Dyn.*, **5**, 441.

Wang, A., X.Zeng, S. S. P.Shen, Q. C.Zeng, and R. E.Dickinson, 2006: Time scales of land surface hydrology. *J. Hydrometeorol.*, **7**, 868–879, https://doi.org/10.1175/JHM527.1.

Williams, A. P., R. E.Schwartz, S.Iacobellis, R.Seager, B. I.Cook, C. J.Still, G.Husak, and J.Michaelsen, 2015: Urbanization causes increased cloud base height and decreased fog in coastal Southern California. *Geophys. Res. Lett.*, **42**, 1527–1536.

Wilson, K., and Coauthors, 2002: Energy balance closure at FLUXNET sites. *Agric. For. Meteorol.*, **113**, 223–243.

Table and Figure Captions (including appendix figures):

Table 1. The difference in leaf wetness [mV] between sunrise and 3-hour after sunrise in three different canopy layers. The positive values indicate the canopy is wetter at around sunrise comparing to 3 hours later.

Table 2. The daytime average of the LH flux $[W\,m^{-2}]$ and CO_2 flux $[\mathrm{mmol}\,m^{-2}\,s^{-1}]$ in CL under foggy and fogless conditions. We only selected the flux data from rainless days. We separated foggy and fogless conditions using visibility data at each time step, and calculated daytime (6:00–18:00) averages of those.

Table 3. The daytime average of the LH flux [W m^{-2}] and CO_2 flux [mmol m^{-2} s^{-1}] in CL under foggy and fogless conditions. We only selected the flux data from rainless days. We separated foggy and fogless conditions using visibility data at each time step, and calculated daytime (6:00–18:00) averages of those.

Fig. 1. (a) The locations of the Chi-Lan (CL) MCF and the Lien-Hua-Chih (LHC) non cloud forest. (b) The frequency of fog occurrence in CL. (b) Comparison of the diurnal cycles in net radiation (Rn $[W\,m^{-2}]$: dashed lines) and latent heat flux (LH flux $[W\,m^{-2}]$: solid lines) between CL (blue lines) and LHC (red lines). The shadings represent the variations in the energy fluxes between the first quartile and the third quartile from 2008 to 2011 (CL) and 2012 to 2013 (LHC), respectively. (c) Comparison of the occurrence probability of the daily maximum net radiation (Rn $[W\,m^{-2}]$: dashed lines) and latent heat flux (LH flux $[W\,m^{-2}]$: solid lines) between CL (blue lines) and

LHC (red lines). The skewness coefficient of Rn in CL is 1.07 and that of LH flux is 2.56. The skewness coefficient of Rn in LHC is -0.63 and that of LH flux is -0.34.

Fig. 2. (a) The comparison of diurnal cycle of latent heat flux $[W/m^2]$ between CL flux tower observation and CLM simulation (CTR). (b) The comparison of latent heat fluxes $[W/m^2]$ between CL flux tower observations and CLM simulation (CTR). The RMSE means the root mean square error.

Fig. 3. The comparison of the diurnal cycle of potential evapotranspiration (PET $[W\ m^{-2}]$: dashed lines) and latent heat flux (LH flux $[W\ m^{-2}]$: solid lines) between CL (Chi-Lan: blue lines) and LHC (Lien-Hua-Chih: red lines). The shading color represents the variation of the fluxes between the first quartile and the third quartile from four years of data from 2008 to 2011 in CL and two years of data from 2012 to 2013 in LHC.

Fig. 4. The comparison of five meteorological variables obtained from the flux towers between the CL (blue lines) and LHC (red lines) forest: (a) temperature [°C], (b) specific humidity $[g\ kg^{-1}]$ (solid lines) and saturated specific humidity $[g\ kg^{-1}]$ (dashed lines), (c) wind speed $[\mathrm{m\ s^{-1}}]$, and (d) relative humidity [%]. The shadings represent the range of variation of each meteorological variable between the first and the third quartiles of data in CL and LHC.

Fig. 5. (a) Simulations conducted using the Community Land Model V4: with (CTR: blue lines) and without (EXP: orange lines) canopy water representation. (b) Comparison of the diurnal cycle in net radiation $[W\ m^{-2}]$ (dashed lines) and LH flux

$[W\ m^{-2}]$ (solid lines) between CTR and EXP. (c), (d) The partitions of the LH flux (ground evaporation $[W\ m^{-2}]$ (brown lines), transpiration $[W\ m^{-2}]$ (red lines), and canopy evaporation $[W\ m^{-2}]$ (blue lines)) for (c) CTR and (d) EXP. The shadings represent the variations of the energy fluxes between the first quartile and the third quartile from the last eight years of the simulations.

Fig. 6. Schematic plot of the hydro-climatological cycle in the CL MCF.

Fig. 7. (a) The comparison of the diurnal cycle of canopy water [mm] among CTR (blue line), max_cw_0.2 (purple line) and max_cw_0.1 (dark magenta line) and max_cw_0.05 (light magenta line). The shading color represents the variation of the canopy water between the first quartile and the third quartile from the last eight years of each simulation. (b) The comparison of the diurnal cycle of LH fluxes $[W\ m^{-2}]$ among CTR, max_cw_0.2 and max_cw_0.1 and max_cw_0.05. The shading color represents the variation of the canopy water between the first quartile and the third quartile from the last eight years of each simulation. (c) The partition of LH flux among CTR, max_cw_0.2 and max_cw_0.1 and max_cw_0.05. The solid lines, dashed lines and dotted lines represent canopy evaporation$[W\ m^{-2}]$, transpiration$[W\ m^{-2}]$, and ground evaporation$[W\ m^{-2}]$, respectively.

TABLES

Table 1. The difference in leaf wetness [mV] between sunrise and 3-hour after sunrise in three different canopy layers. The positive values indicate the canopy is wetter at around sunrise comparing to 3 hours later.

Height [m]	Difference of leaf wetness between sunrise and 3-hour after sunrise (mean [mV] ± std)
5.3	35.8 ± 67.2*
8.3	75.32 ± 102.44*
11.2	5.05 ± 26.90*
Three-layer averaged	40.59 ± 61.47*
*Significant difference at the 1% significance level (one-tailed t test)	

Table 2. The daytime average of the LH flux $[W\,m^{-2}]$ and CO_2 flux [mmol $m^{-2}\,s^{-1}$] in CL under foggy and fogless conditions. We only selected the flux data from rainless days. We separated foggy and fogless conditions using visibility data at each time step, and calculated daytime (6:00–18:00) averages of those.

	Fogless conditions	Foggy conditions
LH flux $[W\,m^{-2}]$	102.29	45.34
CO_2 flux [mmol $m^{-2}\,s^{-1}$]	-0.0085	-0.0044

Table 3. The daytime average of the LH flux [W m^{-2}] and CO_2 flux [mmol m^{-2} s^{-1}] in CL under foggy and fogless conditions. We only selected the flux data from rainless days. We separated foggy and fogless conditions using visibility data at each time step, and calculated daytime (6:00–18:00) averages of those.

fluxes	seasons	mean of fluxes under fogless conditions	mean of fluxes under foggy conditions	decrement of fluxes in percentage
LH flux [W m^{-2}]	MAM	99.08	49.73	49.81%
	JJA	120.82	55.63	53.96%
	SON	121.28	45.69	62.32%
	DJF	83.99	38.69	53.94%
	annual	102.29	45.34	55.68%
CO_2 flux [mmol m^{-2} s^{-1}]	MAM	-0.0101	-0.0054	46.68%
	JJA	-0.0081	-0.0020	75.27%
	SON	-0.0088	-0.0041	54.1%
	DJF	-0.0078	-0.0045	42.06%
	annual	-0.0085	-0.0044	48.06%

FIGURES

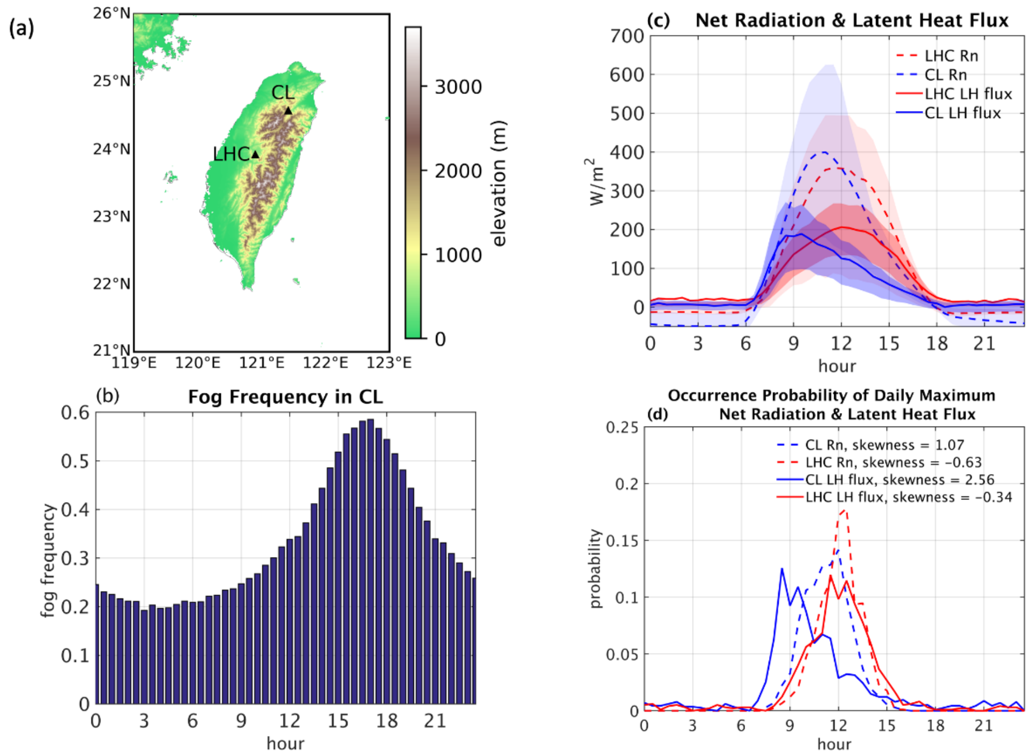

Fig. 1. (a) The locations of the Chi-Lan (CL) MCF and the Lien-Hua-Chih (LHC) non cloud forest. (b) The frequency of fog occurrence in CL. (c) Comparison of the diurnal cycles in net radiation (Rn $[W\ m^{-2}]$: dashed lines) and latent heat flux (LH flux $[W\ m^{-2}]$: solid lines) between CL (blue lines) and LHC (red lines). The shadings represent the variations in the energy fluxes between the first quartile and the third quartile from 2008 to 2011 (CL) and 2012 to 2013 (LHC), respectively. (d) Comparison of the occurrence probability of the daily maximum net radiation (Rn $[W\ m^{-2}]$: dashed lines) and latent heat flux (LH flux $[W\ m^{-2}]$: solid lines) between CL (blue lines) and LHC (red lines). The skewness coefficient of Rn in CL is 1.07 and that of LH flux is 2.56. The skewness coefficient of Rn in LHC is -0.63 and that of LH flux is -0.34.

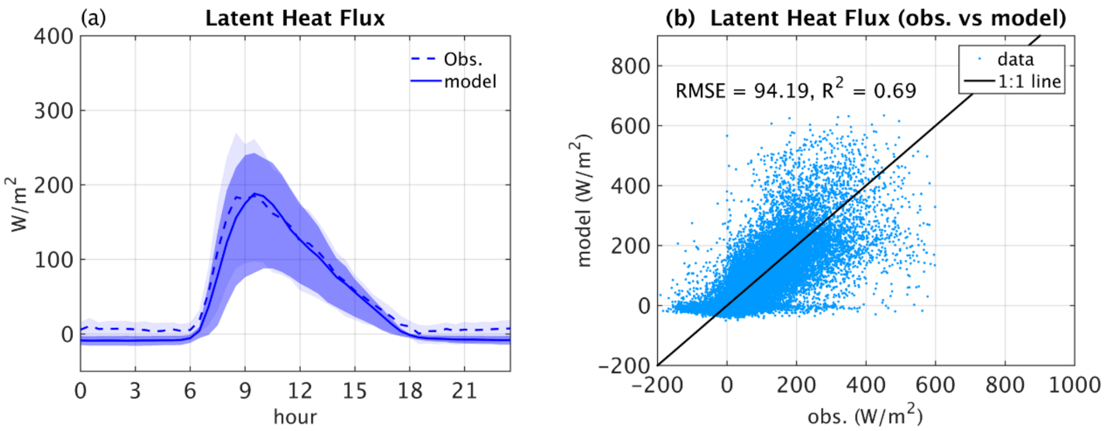

Fig. 2. (a) The comparison of diurnal cycle of latent heat flux $[W/m^2]$ between CL flux tower observation and CLM simulation (CTR). (b) The comparison of latent heat fluxes $[W/m^2]$ between CL flux tower observations and CLM simulation (CTR). The RMSE means the root mean square error.

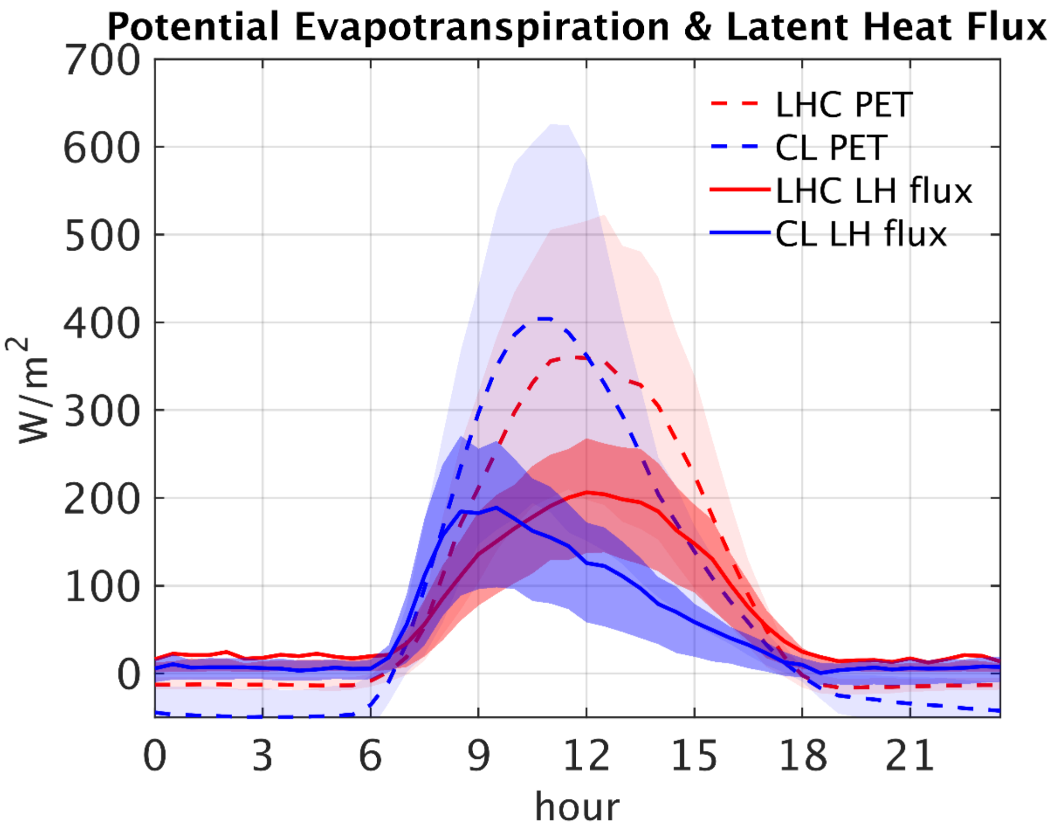

Fig. 3. The comparison of the diurnal cycle of potential evapotranspiration (PET $[W\ m^{-2}]$: dashed lines) and latent heat flux (LH flux $[W\ m^{-2}]$: solid lines) between CL (Chi-Lan: blue lines) and LHC (Lien-Hua-Chih: red lines). The shading color represents the variation of the fluxes between the first quartile and the third quartile from four years of data from 2008 to 2011 in CL and two years of data from 2012 to 2013 in LHC.

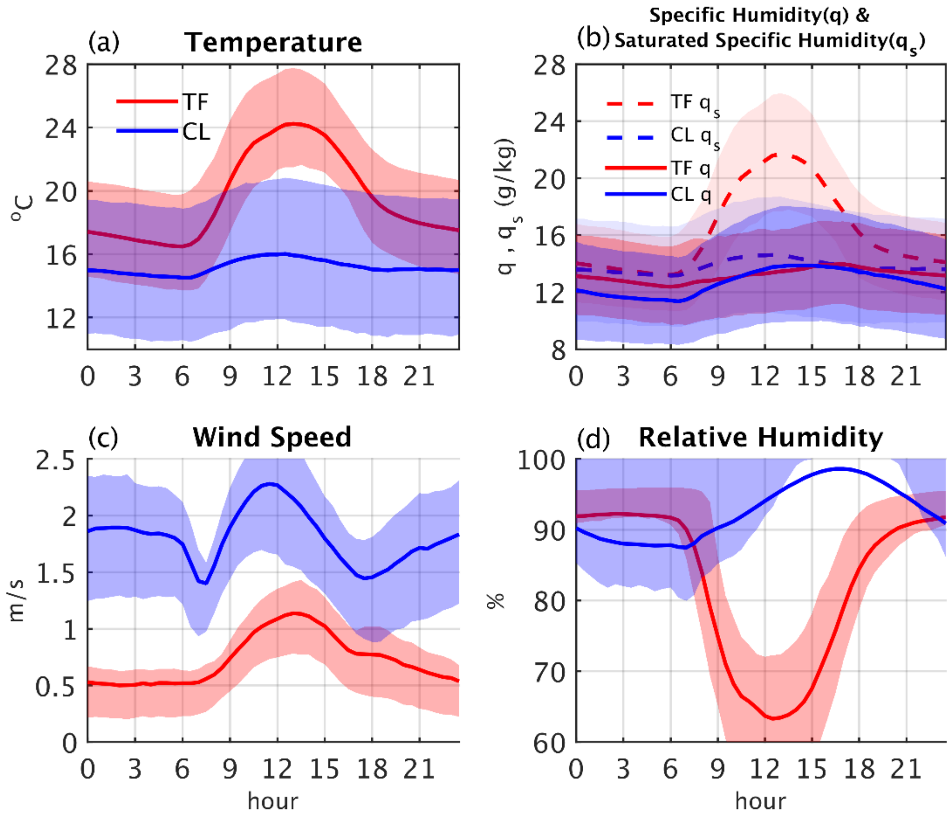

Fig. 4. The comparison of five meteorological variables obtained from the flux towers between the CL (blue lines) and LHC (red lines) forest: (a) temperature [°C], (b) specific humidity [$g\ kg^{-1}$] (solid lines) and saturated specific humidity [$g\ kg^{-1}$] (dashed lines), (c) wind speed [$\mathrm{m\ s^{-1}}$], and (d) relative humidity [%]. The shadings represent the range of variation of each meteorological variable between the first and the third quartiles of data in CL and LHC.

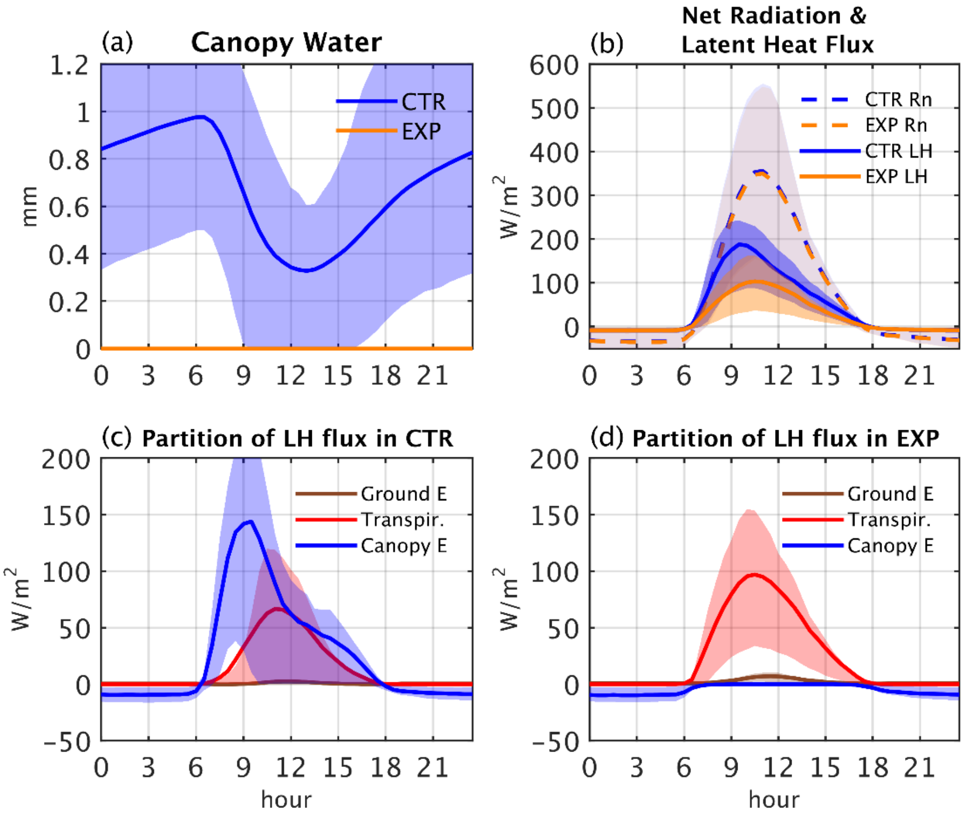

Fig. 5. (a) Simulations conducted using the Community Land Model V4: with (CTR: blue lines) and without (EXP: orange lines) canopy water representation. (b) Comparison of the diurnal cycle in net radiation $[W\ m^{-2}]$ (dashed lines) and LH flux $[W\ m^{-2}]$ (solid lines) between CTR and EXP. (c), (d) The partitions of the LH flux (ground evaporation $[W\ m^{-2}]$ (brown lines), transpiration $[W\ m^{-2}]$ (red lines), and canopy evaporation $[W\ m^{-2}]$ (blue lines)) for (c) CTR and (d) EXP. The shadings represent the variations of the energy fluxes between the first quartile and the third quartile from the last eight years of the simulations.

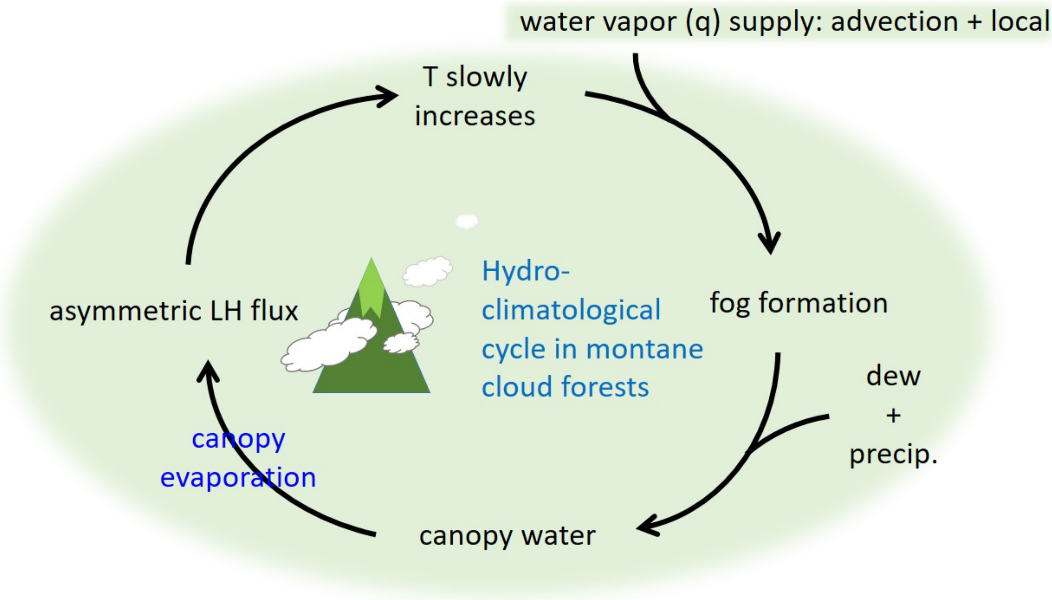

Fig. 6. Schematic plot of the hydro-climatological cycle in the CL MCF.

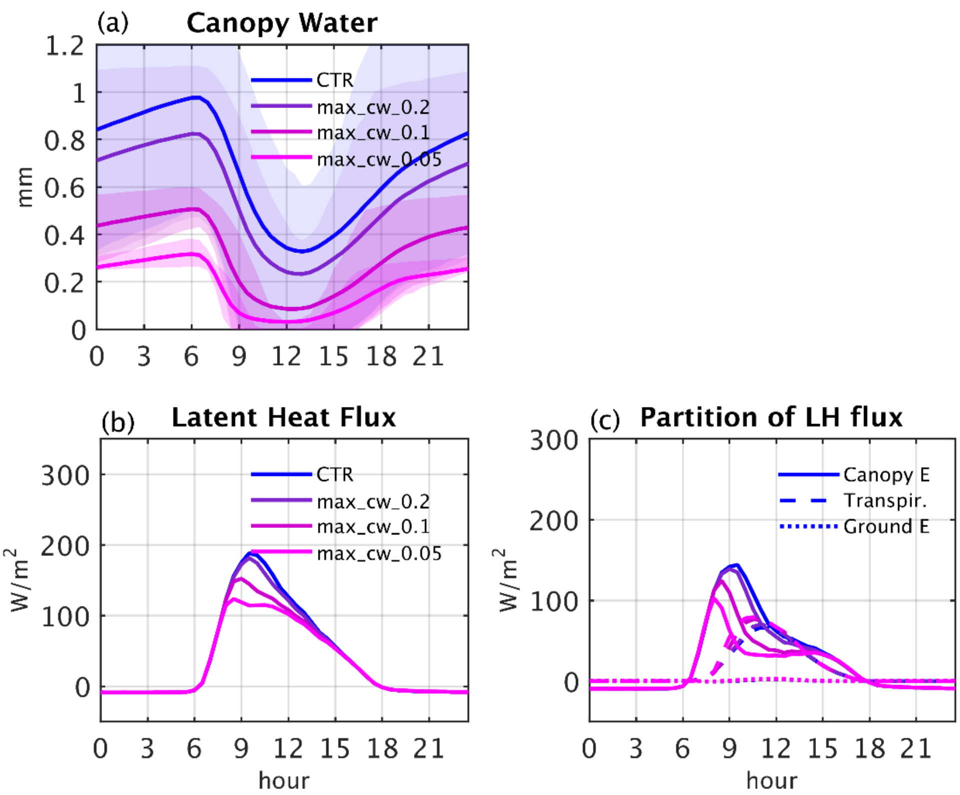

Fig. 7. (a) The comparison of the diurnal cycle of canopy water [mm] among CTR (blue line), max_cw_0.2 (purple line) and max_cw_0.1 (dark magenta line) and max_cw_0.05 (light magenta line). The shading color represents the variation of the canopy water between the first quartile and the third quartile from the last eight years of each simulation. (b) The comparison of the diurnal cycle of LH fluxes $[W\ m^{-2}]$ among CTR, max_cw_0.2 and max_cw_0.1 and max_cw_0.05. The shading color represents the variation of the canopy water between the first quartile and the third quartile from the last eight years of each simulation. (c) The partition of LH flux among CTR, max_cw_0.2 and max_cw_0.1 and max_cw_0.05. The solid lines, dashed lines and dotted lines represent canopy evaporation$[W\ m^{-2}]$, transpiration$[W\ m^{-2}]$, and ground evaporation$[W\ m^{-2}]$, respectively.